Delocalization of the effective interaction for inner-shell ionization in crystals

M. P. Oxley and L. J. Allen
School of Physics, University of Melbourne, Parkville, Victoria 3052, Australia
(Received 14 July 1997; revised manuscript received 26 September 1997)

The delocalization of the effective interaction for inner-shell ionization by electrons in crystals is investigated. In particular K- and L-shell ionization in Mo and GaAs by 400 keV incident electrons is modeled from first principles using Hartree-Fock bound-state wave functions and the results are compared with experimental data in the literature. The delocalization of the effective interaction for L-shell ionization can be substantially different from simple estimates of the delocalization used to date. [S0163-1829(98)04706-7]

I. INTRODUCTION

Charged particles incident on a crystal near a crystal axis or parallel to planes in the crystal undergo channeling. One consequence of channeling is a variation in the yield of x rays arising from inner-shell ionization by the charged particles when the orientation of the incident beam is varied. Here we consider this phenomenon for electron induced x-ray production.[1–4] In the early 1980's the orientation dependence of the x-ray yield was applied to determine the site occupancies of cations in spinels.[5,6] The approach was further developed in determining the concentration of substitutional atoms on specific lattice sites by Spence and Taftø,[7–10] the method being dubbed atom location by channeling enhanced microanalysis (ALCHEMI). Many attempts have been made since to refine and improve the ALCHEMI method.[11–18] The crucial point which limits the accuracy of ALCHEMI is a lack of knowledge from first principles of the delocalization of the inner-shell ionization event leading to x-ray production.[16] Approximate ways have been proposed to include delocalization corrections in the ALCHEMI technique[14,19,20] or statistical methods, which are less sensitive to a precise knowledge of the delocalization, have been employed.[12,13,17]

Significant errors can be introduced in ALCHEMI if the atomic inner-shell interaction is treated as perfectly localized (a δ function at the atomic nucleus). Following previous investigations (see papers cited in Ref. 21) the measured x-ray emission rate of elements under systematic row conditions was compared with those based on hydrogenlike and δ-function models for K-shell ionization.[21] The results demonstrated the importance of the delocalization of the interaction. Ionization of light elements is less localized since the inner-shell electrons are distributed at larger distances from the nucleus. Attempts have been made to correct for delocalization based on knowledge of impact parameters.[19,20] The calculations done here, based on Hartree-Fock bound state wave functions, allow us to model the delocalization of the inner-shell ionization interaction in crystals realistically from first principles. Unlike the case of a hydrogenic model[21] (which is only a reasonable approximation for K-shell ionization in heavier elements), these calculations are relatively complex and time consuming. In this paper we present the theoretical details and outcomes of first principles calculations of ionization cross sections for 400 keV electrons incident on Mo and GaAs for both K- and L-shell ionization. We compare our calculations to energy dispersive x-ray (EDX) data, based on inner shell ionization events, taken by Nüchter and Sigle.[16] This allows us to address the issue of the delocalization of the ionization interaction in a fundamental way and to compare the results with recently measured high quality data. Nüchter and Sigle deduced the delocalization from the data in a phenomenological way,[16] but *a priori* knowledge of the delocalization is crucial to obtain accurate quantitative information using the ALCHEMI technique. The ALCHEMI method and its limitations to date have been discussed in some detail by Nüchter and Sigle.[16]

The diffraction of the incident electron modifies the angular distribution of the electron ejected in an ionization event by making it a function of the orientation of the crystal relative to the incident beam, the site of the $(e,2e)$ event in the unit cell and the depth in the crystal. Unlike the free atom case, the phase of the atomic transition matrix element is an essential part of the physics. This is taken into account in a general expression which can model the cross section for any specific type of inelastic scattering (such as inner-shell ionization) in a crystalline environment.[21,22] Besides the contribution from dynamical electrons, this expression takes into account the contribution to the inelastic scattering under consideration from all other (background) inelastic scattering in the crystal leading to absorption from the dynamical Bragg-reflected beams—for example, the contribution due to thermal diffuse scattering (TDS). The cross-section expression is based upon a general nonlocal formulation of scattering.[22,23] Under some circumstances nonlocal effects can be important.[24]

It has been demonstrated[25] why, in EDX spectroscopy, integration over the dynamical states of the inelastically scattered electrons averages in such a way that an effective plane wave representation of the scattered electrons is a good approximation. We will assume that to be the case here.

II. THEORY

A. Inelastic cross sections

An expression for the cross section for inelastic scattering from a crystal of thickness t has recently been derived[22,23] based on the one-particle Schrödinger equation with a non-

local term to represent the absorptive scattering. This result can also be obtained with suitable approximations from the formalism of Dudarev and co-workers.[26] The expression, which implicitly assumes integration over all final states of the scattered electron, is as follows:

$$\sigma = NV_c\left\{\left[1-\sum_{i,j} B^{ij}(t)\sum_{\mathbf{g}} C_{\mathbf{g}}^{i}C_{\mathbf{g}}^{j*}\right]\mu_{\mathbf{0,0}} + \sum_{i,j} B^{ij}(t)\sum_{\mathbf{g},\mathbf{h}} C_{\mathbf{g}}^{i}C_{\mathbf{h}}^{j*}\mu_{\mathbf{h,g}}\right\}, \tag{1}$$

where NV_c is the total crystal volume,

$$B^{ij}(t) = \alpha^i\alpha^{j*}\frac{\exp[i(\lambda^i-\lambda^{j*})t]-1}{i(\lambda^i-\lambda^{j*})t} \tag{2}$$

and the Bloch wave coefficients λ^i in the $B^{ij}(t)$ and the Bloch state amplitudes α^i and coefficients $C_{\mathbf{g}}^{i}$ come from solution of the Bethe scattering equations. The $\mu_{\mathbf{h,g}}$ refer to the specific inelastic scattering under consideration (in this paper inner-shell ionization) and **g** and **h** are reciprocal lattice vectors. It is important to note that while, for our purposes, the $\mu_{\mathbf{h,g}}$ refer to ionization, the Bloch state coefficients $C_{\mathbf{g}}^{i}$ in Eq. (1) and scattering coefficients λ^i in Eq. (2) come from solutions of the total scattering equations[22] and hence in principle include all forms of absorptive scattering concurrently occurring. In particular, the inclusion of TDS is crucially important to obtain accurate cross sections. The first term in Eq. (1) (the factor in square brackets multiplied by $\mu_{\mathbf{0,0}}$) accounts for ionization by electrons which have been ''dechanneled'' or absorbed from the dynamical elastic beams by wide angle (mainly TDS) scattering. The second term represents the dynamical contribution to σ (which is attenuated by the absorptive scattering).

Since Eq. (1) was derived from the Schrödinger equation, the $\mu_{\mathbf{h,g}}$ can readily be related to the coefficients of the nonlocal inelastic scattering potential under consideration via

$$V_{\mathbf{h,g}} = \hbar^2 k_0 \mu_{\mathbf{h,g}}/2m, \tag{3}$$

where k_0 is the wave number of the incoming electrons. The nonlocal nature of the optical potential representing the inelastic scattering is fundamental.[23,24] The nonlocal potential connects the action of volume elements $d\mathbf{r}'$ elsewhere to a point **r** in the crystal. Approximating the nonlocal potential by a local one means that the potential then only depends on the point **r**, which simplifies calculations and makes visualization of the potential more straightforward. An approximate way to localize the inelastic potential for high energy electrons is to assume that $V_{\mathbf{h,g}} \approx V_{\mathbf{h-g,0}}$, which is how the elastic part of the potential is usually approximated (the nonlocal exchange contribution is small). This is a standard approximation[27] which is often made and has been shown to be excellent when applied to EDX (Refs. 21,24,28–30) and Rutherford backscattering.[31] The $\mu_{\mathbf{h,g}}$ are not simply a property of the crystal alone (such as the Fourier coefficients of the elastic potential) but depend on the experimental conditions.

B. The inelastic scattering coefficients for ionization

The inelastic scattering coefficients $\mu_{\mathbf{h,g}}$ in Eq. (1) take the following form for inner-shell ionization:[23]

$$\mu_{\mathbf{h,g}} = \frac{4n\mathcal{F}[\text{site}]}{(2\pi)^3 k_0 V_c a_0^2}\int K'\kappa^2 \times\left[\int\left(\sum_{m_l}\int \frac{F^{\beta*}(\mathbf{Q_h},\boldsymbol{\kappa})F^{\beta}(\mathbf{Q_g},\boldsymbol{\kappa})}{|\mathbf{Q_h}|^2|\mathbf{Q_g}|^2}d\Omega_{\kappa}\right)d\Omega_{K'}\right]d\kappa, \tag{4}$$

where $\boldsymbol{\kappa}$ is the ejected electron wave vector, $\mathcal{F}[\text{site}]$ is the crystallographic site term, and $F^{\beta}(\mathbf{Q_g},\boldsymbol{\kappa})$ the transition matrix element for the atom of species β. The angular range of the scattered electron integration $d\Omega_{K'} = \sin\theta d\theta d\phi$ extends over all space. The range of integration over the magnitude of the ejected electron wave vector is determined by the threshold energy E_t for ionization. The factor n (usually 2) has been included to account for different spin states within each suborbital. The sum over the azimuthal quantum number m_l of the initial bound state is required for other than s orbitals.

The calculation of atomic form factors and inelastic scattering matrix elements for inner-shell ionization within a crystalline environment requires the evaluation of integrals occurring in Eq. (4) of the form

$$I(\mathbf{Q_g},\mathbf{Q_h},\boldsymbol{\kappa}) = \sum_{m_l}\int F^{\beta*}(\mathbf{Q_h},\boldsymbol{\kappa})F^{\beta}(\mathbf{Q_g},\boldsymbol{\kappa})d\Omega_{\kappa}, \tag{5}$$

where $F^{\beta}(\mathbf{Q_h},\boldsymbol{\kappa})$ is an atomic transition matrix element for atom species β given by

$$F^{\beta}(\mathbf{Q_h},\boldsymbol{\kappa}) = \int b^{\beta*}(\boldsymbol{\kappa},\mathbf{r})\exp[i\mathbf{Q_h}\cdot\mathbf{r}]u_0^{\beta}(\mathbf{r})d\mathbf{r}. \tag{6}$$

Here $\mathbf{Q_g} = \mathbf{q}+\mathbf{g}$, with **q** the momentum transfer. Analytic evaluation of Eq. (5) for K-shell ionization using a screened hydrogenic model in a momentum representation has been previously presented.[32] A method for calculating $I(\mathbf{Q_g},\mathbf{Q_h},\boldsymbol{\kappa})$ in an angular momentum representation has been suggested by Saldin and Rez.[33] This method is suitable for more realistic atomic models and is not limited to K-shell ionization and our approach will be similar.

The use of a central potential model results in the following form for the bound-state wave function:

$$u_0^{\beta}(\mathbf{r}) = \frac{1}{r}u_{nl}(r)Y_{lm_l}(\hat{\mathbf{r}}). \tag{7}$$

Here $u_{nl}(r)$ denotes the radial wave function for the orbital specified by the quantum numbers n and l. We use a hat to

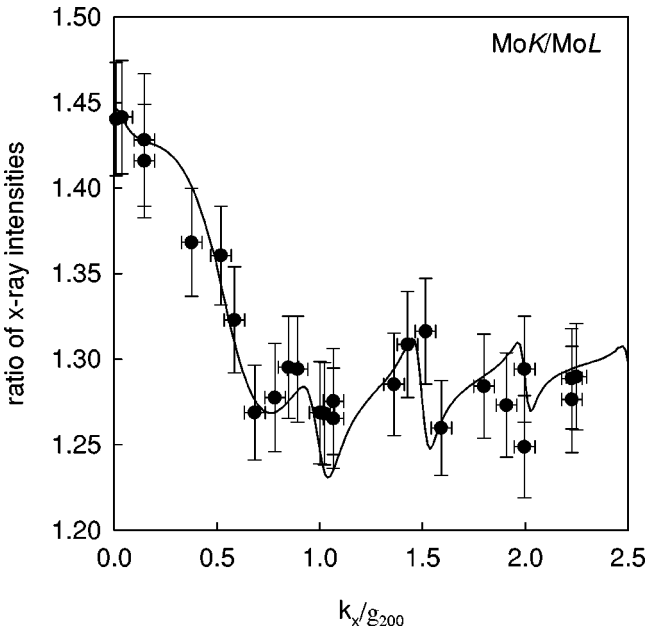

FIG. 1. The ratio of K-shell ionization cross section to L-shell ionization cross section for 400 keV electrons incident on Mo at 300 K as a function of orientation. A value of 0.5 on the x axis (orientation) corresponds to $(\bar{2}\,0\,0)$ being in the exact Bragg orientation. Absorption due to TDS has been included using an Einstein model. An additional mean absorption with a mean free path of 500 Å has been included in the calculations to achieve agreement with the experimental results of Nüchter and Sigle.

denote a unit vector in the argument of the spherical harmonic $Y_{lm_l}(\hat{\mathbf{r}})$. The appropriate form of the continuum wave function is[34]

$$b^{\beta}(\boldsymbol{\kappa},\mathbf{r})=\frac{1}{2\kappa r}\sum_{l'=0}^{\infty} i^{l'}(2l'+1)\exp(i\delta_{l'})u_{\kappa l'}(r)P_{l'}(\hat{\boldsymbol{\kappa}}\cdot\hat{\mathbf{r}}) \quad , \tag{8}$$

where $\delta_{l'}$ is the partial wave phase shift. The continuum wave function is normalized as

$$\int b^{\beta *}(\boldsymbol{\kappa},\mathbf{r})b^{\beta}(\boldsymbol{\kappa}',\mathbf{r})d\mathbf{r}=(2\pi)^3\delta(\boldsymbol{\kappa}'-\boldsymbol{\kappa}), \tag{9}$$

with the radial wave function $u_{\kappa l'}(r)$ satisfying

$$\int u_{\kappa' l'}(r)u_{\kappa l'}(r)dr=2\pi\delta(\kappa'-\kappa). \tag{10}$$

The $u_{\kappa l'}(r)$ are normalized by matching the asymptotic form[34]

$$u_{\kappa l'}(r\rightarrow\infty)=2\sin\left(\kappa r+\frac{1}{\kappa}\ln 2\kappa r-\frac{1}{2}l'\pi+\delta_{l'}\right) \tag{11}$$

to Coulomb functions at a suitably large radius.

Expanding the exponential term in Eq. (6) and the Legendre polynomial in Eq. (8) in spherical harmonics, Eq. (6) can be written in the form

$$\begin{aligned}F^{\beta}(\mathbf{Q_h},\boldsymbol{\kappa})=&\frac{8\pi^2}{\kappa}\sum_{l'=0}^{\infty}\sum_{m_{l'}=-l'}^{l'}(-i)^{l'}\\&\times\exp(-i\delta_{l'})Y_{l'm_{l'}}(\hat{\boldsymbol{\kappa}})\sum_{\lambda=0}^{\infty}\sum_{m_\lambda=-\lambda}^{\lambda}i^{\lambda}Y^{*}_{\lambda m_\lambda}(\hat{\mathbf{Q}}_\mathbf{h})\\&\times\int\frac{1}{r^2}u_{\kappa l'}(r)j_\lambda(Q_\mathbf{h}r)u_{nl}(r)Y^{*}_{l'm_{l'}}(\hat{\mathbf{r}})\\&\times Y_{lm_l}(\hat{\mathbf{r}})Y_{\lambda m_\lambda}(\hat{\mathbf{r}})d\mathbf{r},\end{aligned} \tag{12}$$

where the index λ arises from the expansion for the exponential. Introducing the notation

$$G^{\lambda}_{nl,\kappa l'}(Q_\mathbf{h})=\int u_{\kappa l'}(r)j_\lambda(Q_\mathbf{h}r)u_{nl}(r)dr \tag{13}$$

and using the properties of the spherical harmonics, the atomic transition matrix element can be written in the form

$$\begin{aligned}F^{\beta}(\mathbf{Q_h},\boldsymbol{\kappa})=&\frac{8\pi^2}{\kappa}\sum_{l'=0}^{\infty}\sum_{m_{l'}=-l'}^{l'}(-1)^{m_{l'}}(-i)^{l'}\\&\times\exp(-i\delta_{l'})Y_{l'm_{l'}}(\hat{\boldsymbol{\kappa}})\sum_{\lambda=0}^{\infty}\sum_{m_\lambda=-\lambda}^{\lambda}i^{\lambda}\\&\times Y^{*}_{\lambda m_\lambda}(\hat{\mathbf{Q}}_\mathbf{h})G^{\lambda}_{nl,\kappa l'}(Q_\mathbf{h})\\&\times\left[\frac{(2l'+1)(2\lambda+1)(2l+1)}{4\pi}\right]^{1/2}\begin{pmatrix}l' & \lambda & l\\0 & 0 & 0\end{pmatrix}\\&\times\begin{pmatrix}l' & \lambda & l\\-m_{l'} & m_\lambda & m_l\end{pmatrix}.\end{aligned} \tag{14}$$

The arrays are Wigner $3j$ symbols.

The integral $I(\mathbf{Q_g},\mathbf{Q_h},\boldsymbol{\kappa})$ given by Eq. (4) can now be evaluated using the orthonormality of the spherical harmonics and the orthogonality relations for the $3j$ symbols. We obtain

$$\begin{aligned}I(\mathbf{Q_g},\mathbf{Q_h},\boldsymbol{\kappa})=&\left(\frac{4\pi}{\kappa}\right)^2(2l+1)\sum_{l'=0}^{\infty}(2l'+1)\sum_{\lambda=0}^{\infty}(2\lambda+1)\\&\times G^{\lambda}_{nl,\kappa l'}(Q_\mathbf{h})G^{\lambda}_{nl,\kappa l'}(Q_\mathbf{g})\\&\times\begin{pmatrix}l' & \lambda & l\\0 & 0 & 0\end{pmatrix}^2P_\lambda(\hat{\mathbf{Q}}_\mathbf{h}\cdot\hat{\mathbf{Q}}_\mathbf{g}).\end{aligned} \tag{15}$$

For the diagonal case where $\mathbf{h}=\mathbf{g}$ this reduces to

$$\begin{aligned}I(\mathbf{Q_g},\boldsymbol{\kappa})=&\left(\frac{4\pi}{\kappa}\right)^2(2l+1)\sum_{l'=0}^{\infty}(2l'+1)\sum_{\lambda=0}^{\infty}(2\lambda+1)\\&\times[G^{\lambda}_{nl,\kappa l'}(Q_\mathbf{g})]^2\begin{pmatrix}l' & \lambda & l\\0 & 0 & 0\end{pmatrix}^2.\end{aligned} \tag{16}$$

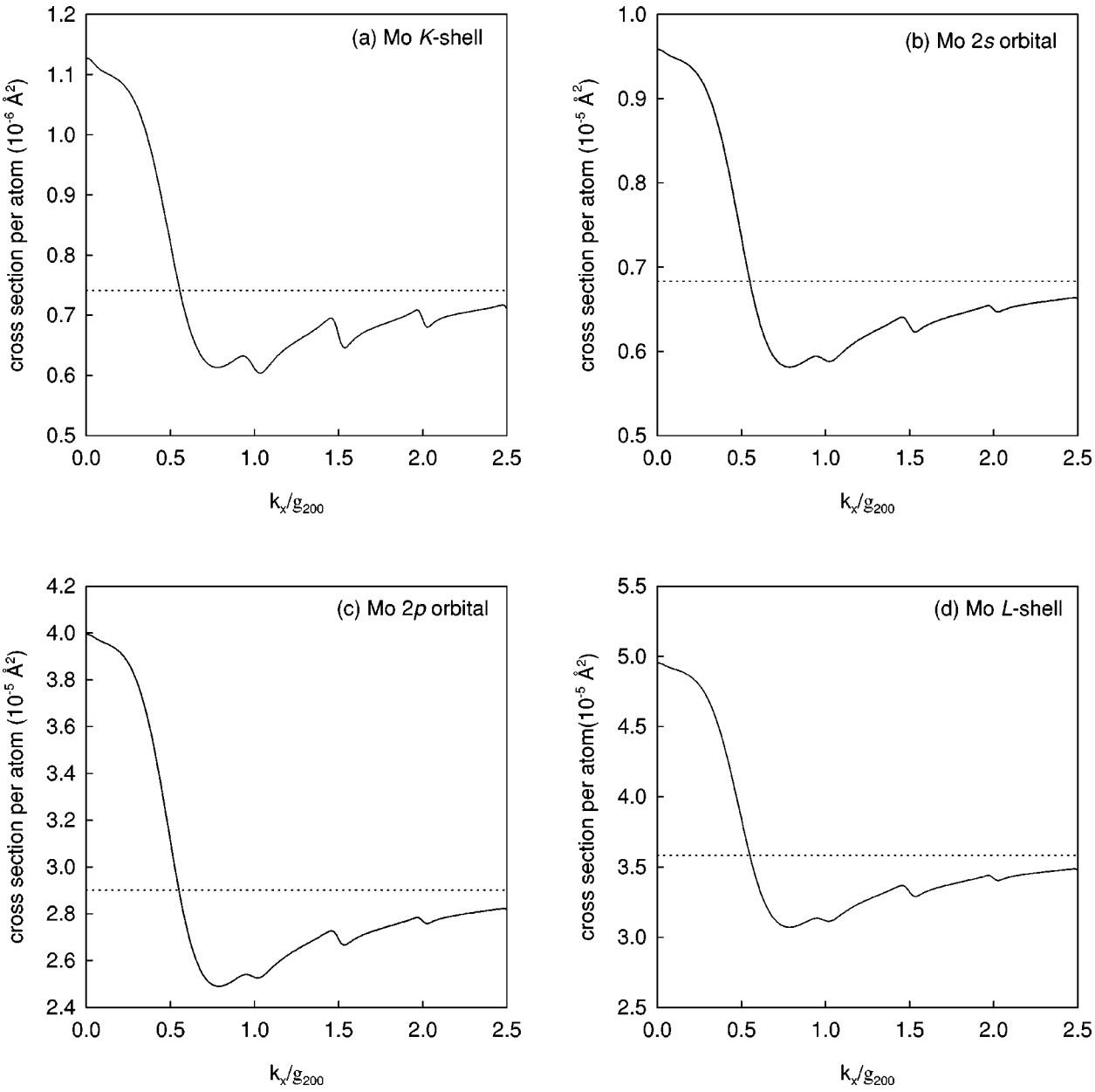

FIG. 2. Ionization cross sections per atom σ for Mo for 400 keV electrons incident on Mo at 300 K shown as a function of orientation. (a) K-shell cross section. (b) Ionization of electrons in the $2s$ orbital. (c) Ionization of electrons in the $2p$ orbital. (d) The total L-shell cross section. The value of the cross section for an isolated atom is shown by the horizontal lines.

III. RESULTS AND DISCUSSION

Our calculations are based on the formalism described in the previous section. Bound-state radial wave functions were calculated using Cowan's program RCN (Ref. 35) which calculates Hartree-Fock wave functions with relativistic corrections. Continuum wave functions were calculated by solving Schrödinger's equation using a Hartree-Slater potential.[35] Calculation of the continuum wave functions describing the ejected electron for kinetic energies of the order of hundreds of keV required careful numerical analysis and extensive stability and accuracy checks have been undertaken. Convergence of all integrations and partial wave summations has been carefully checked.

Data for ratios of x-ray intensities have been taken by Nüchter and Sigle[16] for a {200} sytematic row in Mo and a {400} sytematic row in GaAs. Their samples were wedge shaped and ranged in thickness from 250−1000 Å in the case of Mo and 0−3030 Å in the case of GaAs. The experiments were conducted at room temperature (300 K) and the incoming electrons had an energy of 400 keV.

The ratio of K- to L-shell ionization cross sections for Mo is shown as a function of orientation in Fig. 1. For ease of comparison we have adopted Nüchter and Sigle's notation describing the orientation of the crystal. A value of 0.5 on the orientation axis in the figure corresponds to $(\bar{2}\,0\,0)$ being in the exact Bragg orientation. The results have been averaged over the varying thickness of the wedge by using Eq. (1) and Eq. (2) in integrated form. The results were obtained from a Bloch wave calculation using 11 beams (as described in Refs. 22 and 23) and including absorption due

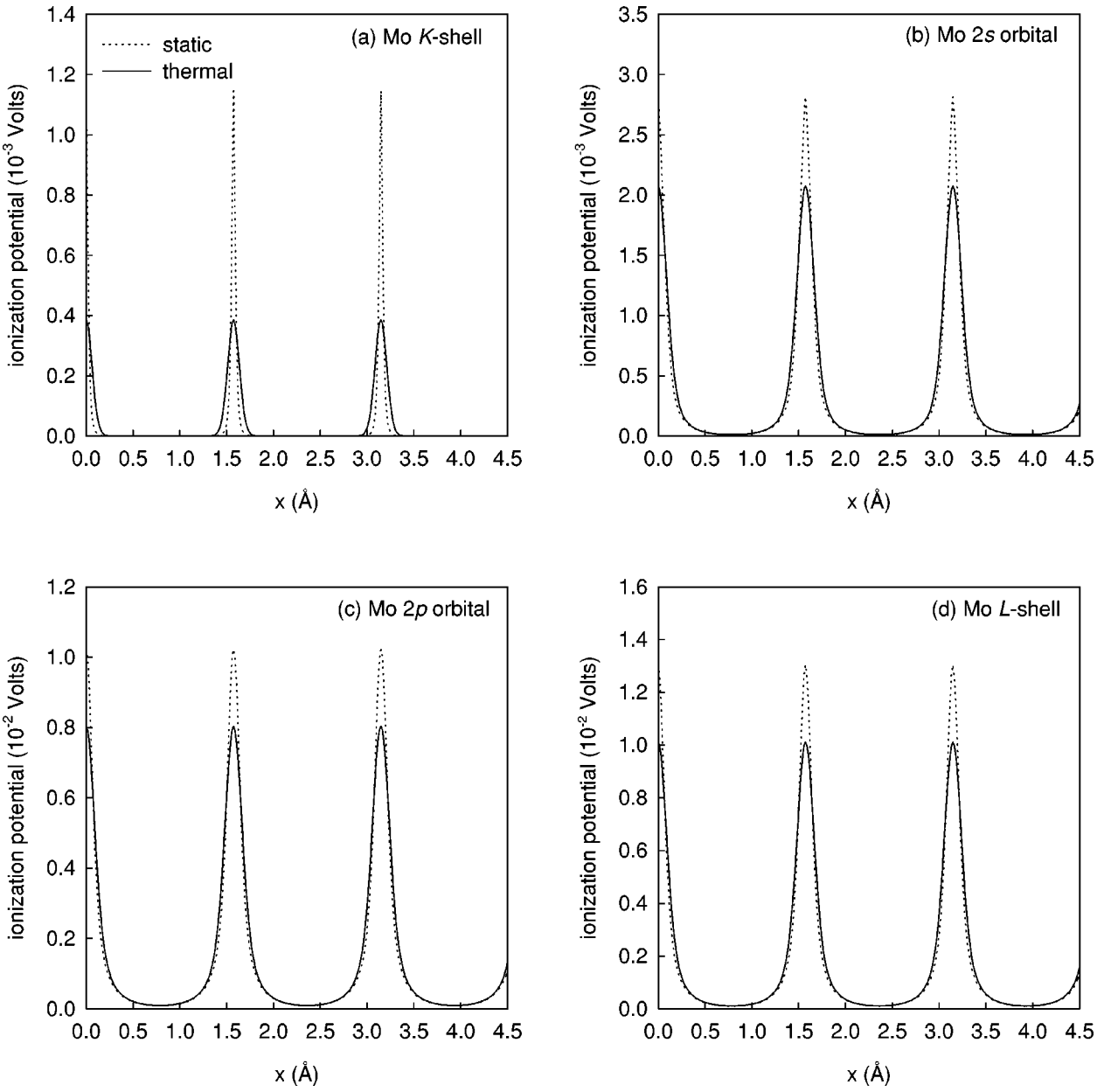

FIG. 3. Projected ⟨200⟩ real space representations of the effective ionization potential pertinent to x-ray emission for 400 keV electrons incident on Mo at 300 K. Both static ionization potentials and those modified by thermal smearing are shown. (a) Potentials for ionization of K-shell electrons. (b) Potentials for ionization of electrons in a $2s$ orbital. (c) Potentials for ionization of electrons in a $2p$ orbital. (d) The total potential for the ionization of L-shell electrons.

to TDS calculated from an Einstein model.[36–38] An additional mean absorption with a mean free path of 500 Å has been included in the calculations to achieve the close agreement with the experimental x-ray emission results of Nüchter and Sigle shown in the diagram. The additional absorption accounts for processes other than TDS which remove electrons from the dynamical beams. All other aspects of the calculation are from first principles. It is tacitly assumed that the total cross section for all (allowed) x-ray emission events corresponding to filling a hole in the K or L shell is proportional to the corresponding total K- or L-shell ionization cross section.

In Fig. 2. we show ionization cross sections per atom σ for Mo as a function of orientation for K and L shells (and the related orbitals) used to calculate the ratio in Fig. 1. The contribution to the total L-shell cross section from the $2p$ orbital is roughly four times that of the $2s$ orbital. The value of the cross section for a free atom is shown by the horizontal lines.

We show the projected real space representation of the effective ionization potential along ⟨200⟩ pertinent to x-ray emission for 400 keV electrons incident on Mo at 300 K in Fig. 3. Both static ionization potentials and those modified by thermal smearing are shown. (Thermal smearing has been included in our cross section calculations). The thermal smearing has been included by means of a Debye-Waller factor in the Fourier coefficients of the ionization potential.[28] We have used a temperature factor $B=0.250$ Å^2. To ensure a completely converged representation of the potential, we used 200 Fourier coefficients for the K-shell case. The more

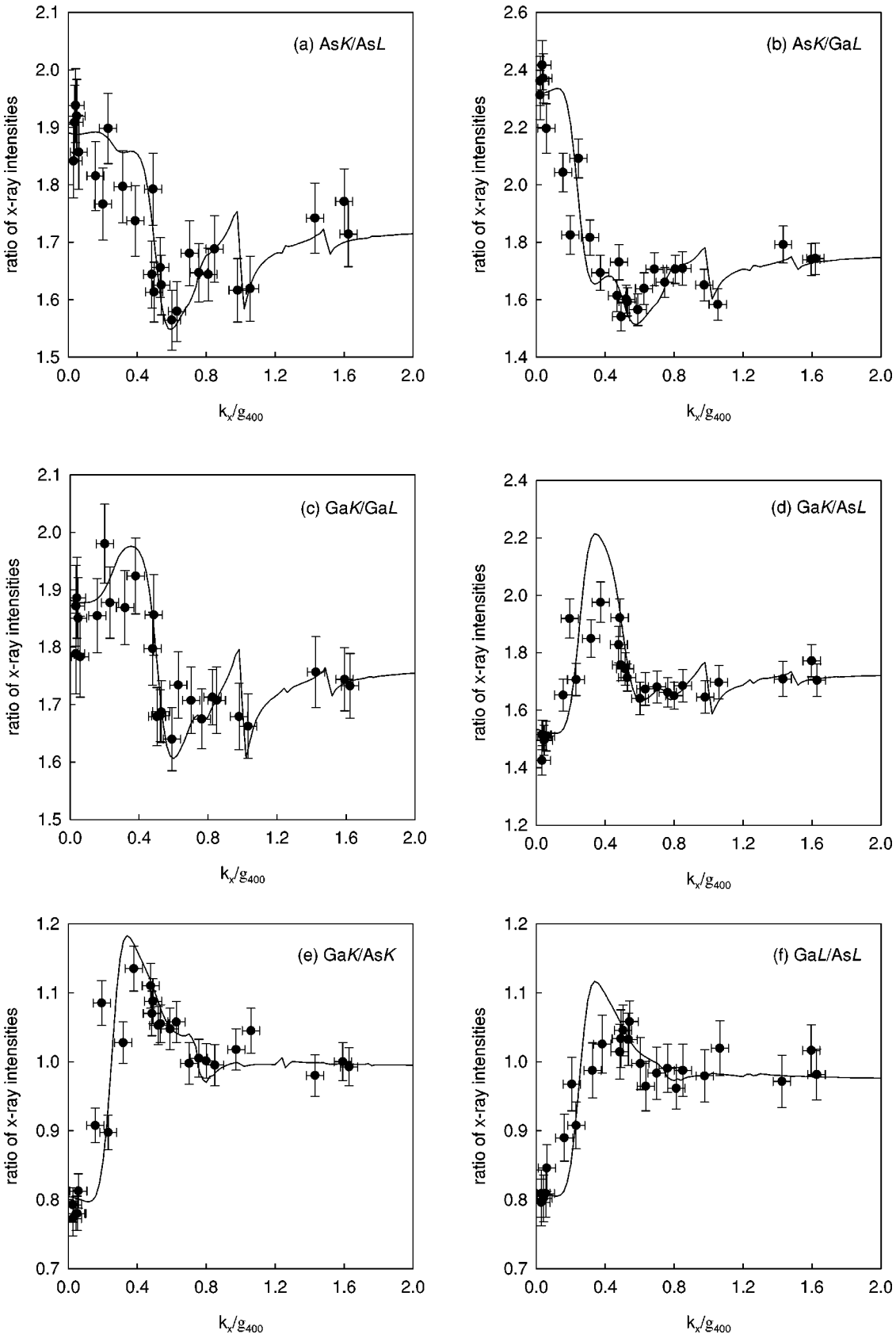

FIG. 4. Ratios of ionization cross sections for 400 keV electrons incident on GaAs at 300 K as a function of orientation. A value of 0.5 on the x axis (orientation) corresponds to $(\bar{4}\,0\,0)$ being in the exact Bragg orientation. Absorption due to TDS has been included using an Einstein model. An additional mean absorption with a mean free path of 1800 Å has been included in the calculations to achieve agreement with the experimental results of Nüchter and Sigle shown in the figures. (a) Ratio of As K-shell cross section to As L-shell cross section (abbreviated AsK/AsL). (b) AsK/GaL. (c) GaK/GaL. (d) GaK/AsL. (e) GaK/AsK. (f) GaL/AsL.

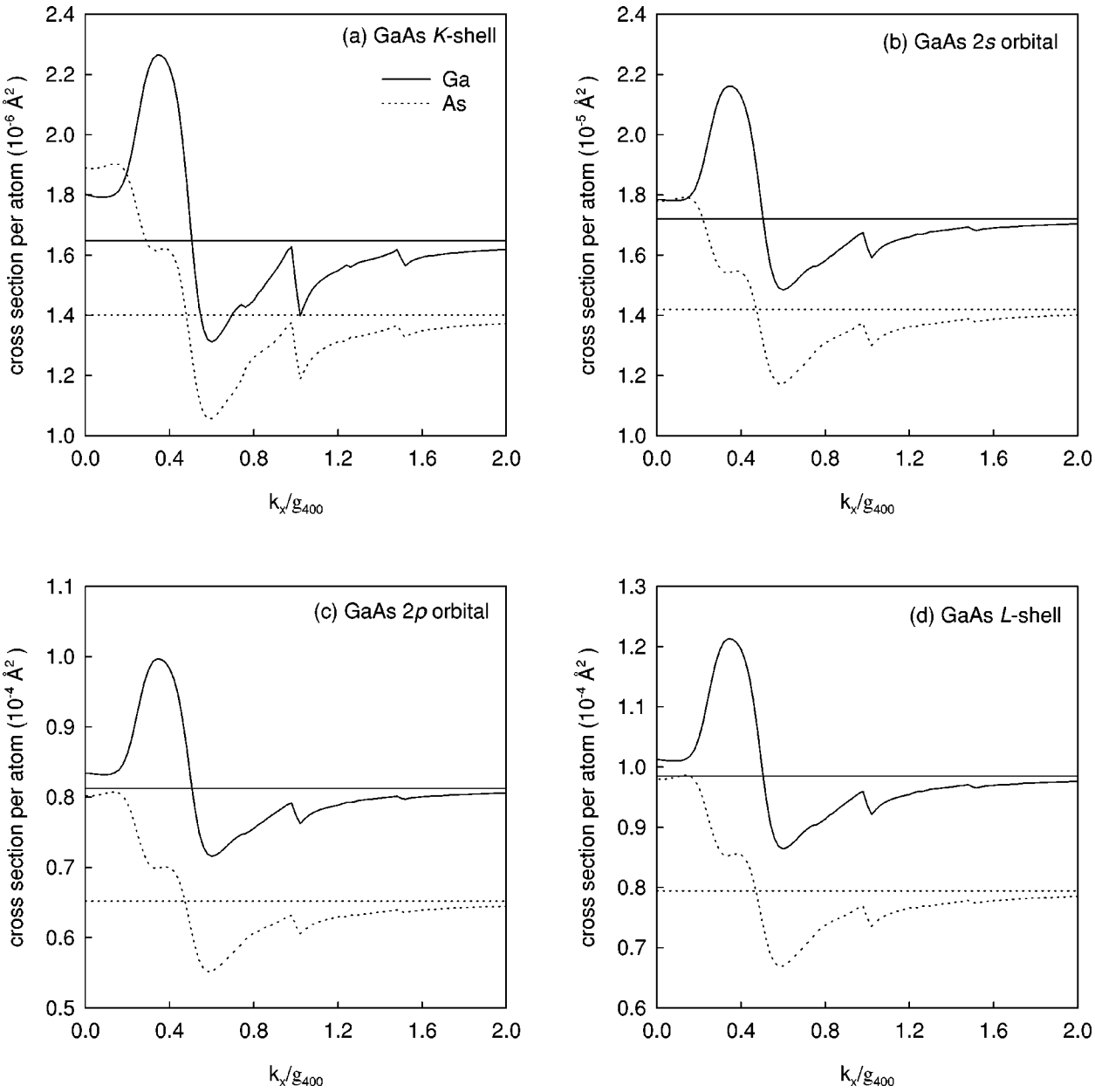

FIG. 5. Ionization cross sections σ per atom for each of the constituents of GaAs for 400 keV incident electrons at 300 K shown as a function of orientation. (a) K-shell cross section. (b) Ionization of electrons in the $2s$ orbital. (c) Ionization of electrons in the $2p$ orbital. (d) The total L-shell cross section. The values of the cross sections for isolated atoms are also shown by the horizontal lines.

delocalized L-shell potentials were calculated using 100 Fourier coefficients. The more localized the static ionization potential, the more significant the effect of thermal smearing so that the K-shell ionization potential is significantly broadened by thermal smearing. The maximum value of the potential for ionization from the $2s$ orbital is approximately twice as large as that for ionization from the $1s$ orbital. However, the thermally smeared $1s$ potential has a maximum value less than a quarter that of the $2s$ potential and the delocalization has more obviously been increased by thermal smearing. The total L-shell ionization potential is an order of magnitude bigger than the K-shell potential and the increased delocalization of the L-shell interaction relative to the K shell is obvious. Most of the contribution to the L-shell potential comes from the $2p$ orbital. The potentials are calculated using Eqs. (3) and (4) and using the approximation $\mu_{\mathbf{h},\mathbf{g}} \approx \mu_{\mathbf{h}-\mathbf{g},\mathbf{0}}$. The validity of this approximation has been checked and is excellent. As expected, the K-shell potential is very similar to that obtained using a screened hydrogenic model.[32]

As can be seen in Table I the half width at half maximum (HWHM) of the thermally smeared K-shell potential is 0.074 Å compared to 0.117 Å for the (total) L-shell potential. The HWHM is directly related to the root-mean-square impact parameter b for the case of a Lorentzian or a Gaussian potential as used by Nüchter and Sigle.[16] On this basis we compare half widths at half maximum with impact parameters in Table I. The (static) impact parameters of Nüchter and Sigle are closer to the estimates given by Pennycook[20] for electron-energy loss spectroscopy (EELS) rather than to

TABLE I. Half widths at half maximum or impact parameters for Mo in Å.

	$1s$ (K shell)	$2s$	$2p$	$2s+2p$ (L shell)
Pennycook				
(static EELS)	0.039	0.223	0.248	0.242
(static EDX)	0.020	0.091	0.100	0.098
Nüchter and Sigle				
(static)	0.058			0.192
(thermal smearing)	0.088			0.203
This work				
(static)	0.022	0.078	0.085	0.084
(thermal smearing)	0.074	0.113	0.118	0.117

those given by the same author for EDX. Our (static) K- and L-shell results are within about 11% of Pennycook's EDX estimates for the impact parameter. It is interesting to note that when convoluted with the contribution from thermal smearing, the Gaussian used by Nüchter and Sigle gave a potential with a delocalization similar to our thermally smeared result.

We show ratios of ionization cross sections for the constituents of GaAs in Fig. 4. A value of 0.5 on the orientation axis in the figure corresponds to $(\overline{4}\,0\,0)$ being in the exact Bragg orientation. Once again the results have been thickness averaged. We used 15 beams in the calculation and, as before, absorption due to TDS was included using an Einstein model. An additional mean absorption with a mean free path of 1800 Å has been included in all the calculations, as this gave the best overall agreement with the experimental data of Nüchter and Sigle.

Shown in Fig. 5. are ionization cross sections per atom σ for both Ga and As as a function of orientation for K and L shells (and the related orbitals) used to calculate the ratios in Fig. 4. The contribution to the total L-shell cross section from the $2p$ orbital is again roughly four times that of the $2s$ orbital. The values of the cross section per atom for scattering from a free atom are shown by the horizontal lines. Thermal smearing has been included using temperature factors $B=0.648$ Å^2 and $B=0.696$ Å^2 for Ga and As, respectively.

As can be seen in Table II the HWHM of the thermally smeared Ga(As) K-shell potential is 0.118 Å(0.121 Å) compared to 0.189 Å(0.183 Å) for the total L-shell potential. Our static values for the HWHM can be compared to those found from Pennycook's expressions[20] given for both EDX and EELS and with those deduced from experiment by Nüchter and Sigle.[16] For the K-shell case, the impact parameter from Pennycook's EDX formula for Ga(As) is within 3%(7%) of our calculated value. However, the Nüchter and Sigle results are substantially different to our results for the static case. When thermal smearing is included then their results and ours are in better agreement, especially in the case of As.

TABLE II. Half widths at half maximum or impact parameters for GaAs in Å.

	$1s$ (K shell)	$2s$	$2p$	$2s+2p$ (L shell)
Ga				
Pennycook				
(static EELS)	0.070	0.457	0.521	0.505
(static EDX)	0.032	0.175	0.198	0.192
Nüchter and Sigle				
(static)	0.132			0.354
(thermal smearing)	0.170			0.370
This work				
(static)	0.033	0.116	0.133	0.129
(thermal smearing)	0.118	0.178	0.192	0.189
As				
Pennycook				
(static EELS)	0.062	0.394	0.447	0.434
(static EDX)	0.029	0.152	0.172	0.167
Nüchter and Sigle				
(static)	0.056			0.290
(thermal smearing)	0.124			0.310
This work				
(static)	0.031	0.107	0.121	0.118
(thermal smearing)	0.121	0.174	0.186	0.183

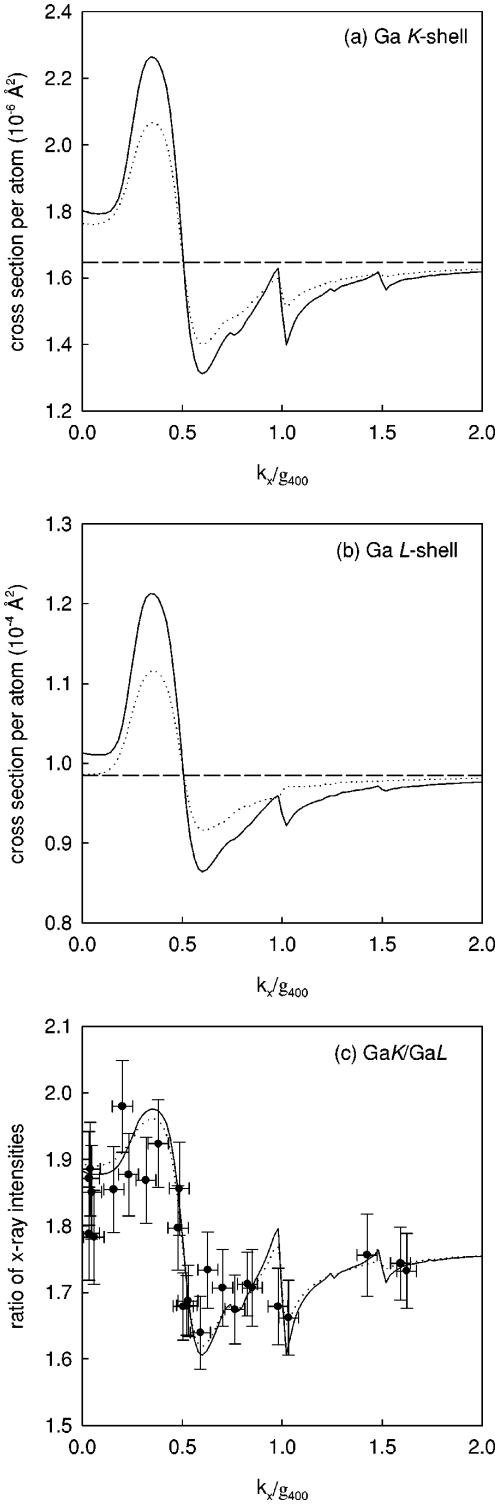

FIG. 6. Cross sections per atom σ for ionization of Ga in GaAs for 400 keV incident electrons at 300 K shown as a function of orientation and compared to those of Nüchter and Sigle. (a) Ga K-shell cross section. (b) Ga L-shell cross section. (c) Ratio of Ga K-shell cross section to Ga L-shell cross section. The values of the cross sections for isolated atoms are also shown.

The effect of thermal smearing on the static ionization potential depends not only on the degree of localization, but also on the shape of the static potential. Here we also see that the thermal smearing does not affect the L-shell potentials as much as the K-shell results. Pennycook's L-shell impact parameters are roughly 50% larger than those calculated here. (Contrast this with the result for the more localized Mo L shell, where the agreement was much better.) Nüchter and Sigle's L-shell parameters are roughly a factor of 2 larger than our calculated values.

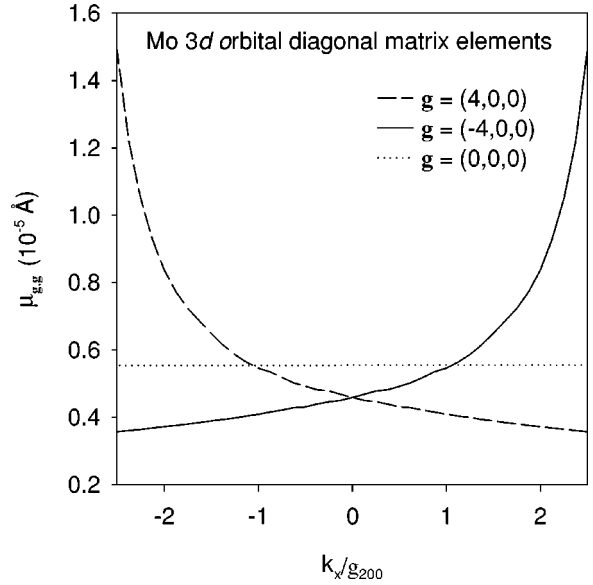

FIG. 7. Diagonal ionization scattering matrix elements $\mu_{\mathbf{g},\mathbf{g}}$ for 400 keV incident electrons at 300 K for ionization of electrons from the $3d$ orbital in Mo.

In Fig. 6. we compare the cross section per atom σ for both K- and L-shell ionization for Ga in GaAs and the resulting ratio of x-ray intensities, calculated from first principles and using Nüchter and Sigle's impact parameter values. Nüchter and Sigle's values are reproduced using, as they did, a Gaussian form of the potential and a proportional model for TDS. Our results are calculated using the much more realistic Einstein model for TDS (Refs. 36–38) and an additional mean free path for absorption of 1800 Å is included to provide the best fit to the experimental data. The values of the cross sections for isolated atoms are also shown. Theoretical values are averaged over thickness and scaled appropriately to fit the experimental single ratios. Theoretical values are calculated using 15 beams. It should be noted that although Nüchter and Sigle's calculations provide a good fit to the experimental ratios, their predicted cross sections for both K- and L-shell ionization are too delocalized.

This investigation has focused on EDX based on K- and L-shell ionization where the assumption that $U_{\mathbf{h},\mathbf{g}}$ is independent of orientation and can be approximated by $U_{\mathbf{h},\mathbf{g}} \approx U_{\mathbf{h}-\mathbf{g},\mathbf{0}}$ is a good one for these rather localized ionization events and the electrons are relatively tightly bound. Where this is not the case, either or both of these assumptions may not be valid. A full nonlocal calculation of the ionization potential coefficients from first principles must then be done. As an example of this we show, in Fig. 7, the variation with orientation of several diagonal ionization matrix elements $\mu_{\mathbf{g},\mathbf{g}}$ for ionization from the $3d$ orbital of Mo. For this more delocalized, low threshold energy interaction, a variation in some of the matrix elements by a factor of 3 is evident (over the range of orientations considered). For a given orientation

the validity of the local approximation would require $U_{\mathbf{g},\mathbf{g}} \approx U_{\mathbf{0},\mathbf{0}}$. This requirement is clearly also not met.

IV. CONCLUSIONS

We have presented theory and calculations which show that the delocalization of the effective interaction for inner-shell ionization in a crystalline environment can be calculated from first principles using realistic Hartree-Fock wave functions. For more delocalized interactions, the results obtained can be substantially different from those obtained using simpler estimates of impact parameters. Successful quantitative application of the ALCHEMI technique requires reliable knowledge of the delocalization of the effective ionization interaction.

ACKNOWLEDGMENTS

We would like to thank Dr. C. J. Rossouw and Dr. T. W. Josefsson for useful discussions on this work. We thank Dr. W. Nüchter and Dr. W. Sigle for sending us their experimental data in tabulated form. L.J.A. acknowledges financial support from the Australian Research Council.

[1] P. Duncumb, Philos. Mag. **7**, 2101 (1962).
[2] C. R. Hall, Proc. R. Soc. London, Ser. A **295**, 140 (1966).
[3] D. Cherns, A. Howie, and M. H. Jacobs, Z. Naturforsch. A **28A**, 565 (1973).
[4] A. J. Bourdillon, P. G. Self, and W. M. Stobbs, Philos. Mag. A **44**, 1335 (1981).
[5] J. Taftø, J. Appl. Crystallogr. **15**, 378 (1981).
[6] J. Taftø and Z. Lilienthal, J. Appl. Crystallogr. **15**, 260 (1982).
[7] J. C. H. Spence and J. Taftø, in *Scanning Electron Microscopy/1982*, edited by O. Johari (SEM, Chicago, 1982), p. 523.
[8] J. Taftø and J. C. H. Spence, Science **218**, 40 (1982).
[9] J. Taftø and J. C. H. Spence, Ultramicroscopy **9**, 243 (1982).
[10] J. C. H. Spence and J. Taftø, J. Microsc. **130**, 147 (1983).
[11] K. M. Krishnan, Ultramicroscopy **24**, 125 (1988).
[12] C. J. Rossouw, P. S. Turner, T. J. White, and A. J. O'Connor, Philos. Mag. Lett. **60**, 225 (1989).
[13] P. S. Turner, T. J. White, A. J. O'Connor, and C. J. Rossouw, J. Microsc. **162**, 369 (1991).
[14] Z. Horita, Philos. Mag. A **67**, 425 (1993).
[15] Z. Horita, H. Kuninaka, T. Sano, M. Nemoto, and J. C. H. Spence, Philos. Mag. A **67**, 425 (1995).
[16] W. Nüchter and W. Sigle, Philos. Mag. A **71**, 165 (1995).
[17] C. J. Rossouw, C. T. Forwood, M. A. Gibson, and P. R. Miller, Philos. Mag. A **74**, 57 (1996).
[18] Z. Horita, M. R. McCartney, and H. Kuninaka, Philos. Mag. A **75**, 153 (1997).
[19] S. J. Pennycook and J. Narayan, Phys. Rev. Lett. **54**, 1543 (1985).
[20] S. J. Pennycook, Ultramicroscopy **26**, 239 (1988).
[21] L. J. Allen and C. J. Rossouw, Phys. Rev. B **47**, 2446 (1993).
[22] L. J. Allen and T. W. Josefsson, Phys. Rev. B **52**, 3184 (1995).
[23] L. J. Allen and T. W. Josefsson, Phys. Rev. B **53**, 11 285 (1996).
[24] L. J. Allen, D. C. Bell, T. W. Josefsson, A. E. C. Spargo, and S. L. Dudarev, Phys. Rev. B **56**, 9 (1997).
[25] T. W. Josefsson and L. J. Allen, Phys. Rev. B **53**, 2277 (1996).
[26] S. L. Dudarev, L.-M. Peng, and M. J. Whelan, Phys. Rev. B **48**, 13 408 (1993).
[27] H. Yoshioka, J. Phys. Soc. Jpn. **12**, 618 (1957).
[28] L. J. Allen and C. J. Rossouw, Phys. Rev. B **42**, 11 644 (1990).
[29] L. J. Allen, T. W. Josefsson, and C. J. Rossouw, Ultramicroscopy **55**, 258 (1994).
[30] T. W. Josefsson, L. J. Allen, P. R. Miller, and C. J. Rossouw, Phys. Rev. B **50**, 6673 (1994).
[31] C. J. Rossouw, P. R. Miller, T. W. Josefsson, and L. J. Allen, Philos. Mag. A **70**, 985 (1994).
[32] V. W. Maslen, J. Phys. B **16**, 2065 (1983).
[33] D. K. Saldin and P. Rez, Philos. Mag. B **55**, 481 (1987).
[34] L. D. Landau and E.M. Lifshitz, *Quantum Mechanics*, 3rd ed. (Permagon, Oxford, 1977).
[35] R. D. Cowan, *The Theory of Atomic Structure and Spectra* (University of California Press, Berkeley, 1981).
[36] C. R. Hall and P. B. Hirsch, Proc. R. Soc. London, Ser. A **286**, 158 (1965).
[37] C. J. Humphreys and P. B. Hirsch, Philos. Mag. **18**, 115 (1968).
[38] L. J. Allen and C. J. Rossouw, Phys. Rev. B **39**, 8313 (1989).